Tailoring the phase transition from topological superconductor to trivial superconductor induced by magnetic textures of a spin chain on a *p*-wave superconductor

Pritam Chatterjee [1,2,*] Saurabh Pradhan [3,†] Ashis K. Nandy [4,‡] and Arijit Saha [1,2,§]

[1]*Institute of Physics, Sachivalaya Marg, Bhubaneswar-751005, India*
[2]*Homi Bhabha National Institute, Training School Complex, Anushakti Nagar, Mumbai 400094, India*
[3]*Lehrstuhl für Theoretische Physik II, Technische Universität Dortmund Otto-Hahn-Str. 4, 44221 Dortmund, Germany*
[4]*School of Physical Sciences, National Institute of Science Education and Research, An OCC of Homi Bhabha National Institute, Jatni 752050, India*

(Received 7 July 2022; revised 3 February 2023; accepted 13 February 2023; published 21 February 2023)

We theoretically investigate the phase transition from a nontrivial topological *p*-wave superconductor to a trivial *s*-wave-like superconducting phase through a gapless phase, driven by different magnetic textures as a one-dimensional spin-chain impurity, e.g., Bloch-type, in-plane, and out-of-plane Néel-type spin chains, etc. In our proposal, the chain of magnetic impurities is placed on a spin-triplet *p*-wave superconductor where we obtain numerically as well as analytically an effective *s*-wave-like pairing due to spin rotation, resulting in gradual destruction of the Majorana zero modes present in the topological superconducting phase. In particular, when the impurity spins are antiferromagnetically aligned, i.e., spiral wave vector $G_s = \pi$, the system becomes an effective *s*-wave superconductor without Majorana zero modes in the local density of states. The Shiba bands, on the other hand, formed due to the overlapping of Yu-Shiba-Rusinov states play a crucial role in this topological to trivial superconductor phase transition, confirmed by the sign change in the minigap within the Shiba bands. We also characterize this topological phase transition via gap closing and winding number analysis. Moreover, interference of the Shiba bands exhibiting oscillatory behavior within the superconducting gap $-\Delta_p$ to Δ_p, as a function of G_s, also reflects an important evidence for the formation of an effective *s*-wave pairing. Such oscillation is absent in the *p*-wave regime. We also analyze the case of two-dimensional *p*-wave superconductor hosting Majorana edge modes (in absence of any magnetic chain) and show that initially Majorana zero modes (in presence of one-dimensional magnetic chain) can hybridize with such Majorana edge modes. Interestingly, in the topological regime with a fixed G_s value, the Mazorana zero modes survive at the ends of the magnetic chain even when the Majorana edge states disappear at some critical value of the chemical potential and exchange coupling strength.

DOI: 10.1103/PhysRevB.107.085423

I. INTRODUCTION

Topological phases of matter have been at the forefront of research in modern condensed matter physics for the past few decades. Due to nonlocal properties of these phases it is not possible to characterize the state of matter with a single physical order parameter. Instead, we need to define a topological invariant which can only take some discrete integer values. Quantization of the Hall conductance was the first signature of nontrivial topological states of matter [1]. However, the theoretical and experimental discovery of the quantum spin Hall effect in two-dimensional (2D) systems [2–6] characterized by $\mathcal{Z}_2$ topological invariant [7,8] have attracted a great deal of attention for the last two decades. These concepts have also been extended to three-dimensional (3D) materials with nontrivial topological features in the band structures [9–17] The above ideas of topology were restricted to the system with a band gap and as a result these systems were insulators. However, later it was realized that the topological classification is in principle valid for a many-body state with a band gap in the spectrum [18]. In this regard, Kitaev's elegant model was developed to characterize the topological superconductor (TSC) for a one-dimensional (1D) system [19,20]. Earlier, Read and Green proposed the idea of TSC in fractional quantum Hall state based on a 2D system [21]. Later on, Fu and Kane emphasized the realization of TSC on the 2D surface of a 3D topological insulator, in close proximity to an *s*-wave superconductor and magnetic insulator [22].

Intriguingly, these TSCs host Majorana zero modes (MZMs) which are of their own antiparticle and satisfy non-Abelian statistics [23–26]. These MZMs are also suggested to be beneficial for topological quantum computation as they are free from decoherence by the environment [26]. In this context, theoretical proposals [27,28] to engineer such a TSC from a semiconducting 1D nanowire with Rashba spin-orbit coupling have stimulated a lot of recent exciting experiments towards realizing this exotic phase hosting MZMs. The zero-bias peak, observed in several transport experiments based

*pritam.c@iopb.res.in
†saurabh.pradhan@tu-dortmund.de
‡aknandy@niser.ac.in
§arijit@iopb.res.in

on hybrid superconductor-semiconductor systems, has been interpreted as the indirect signatures of Majorana fermions [29–34]. However, this conclusion still remains openly debated.

In recent times, much attention has been directed at an alternative proposal, where a TSC phase can be realized in a chain of magnetic impurities placed on the surface of an *s*-wave superconductor [35–54]. Physically, magnetic impurities placed on a conventional superconductor give rise to Yu-Shiba-Rusinov (YSR) states [55–58]. The individual localized YSR states can hybridize and form a band called Shiba band. The helical spin texture plays the combined role of the spin-orbit coupling and external magnetic field in the 1D nanowire proposal [27,28]. As a result, the topological superconducting phase can be effectively realized in the Shiba bands, akin to spinless *p*-wave superconductors (Kitaev model) hosting MZMs at the two ends of the 1D spin chain [19,59–61]. A particular advantage of the YSR chain proposal is that the signature of YSR states or topological MZMs can be experimentally detected by scanning tunneling microscopy (STM) measurements [62–66].

In our work, we take the opposite route in which a chain of magnetic impurities is placed on a spin-triplet *p*-wave superconducting substrate. Although (pseudo)spin-triplet or odd-parity superconductors are rarely observed in nature, various successful attempts are made to host unconventional superconductivity in materials, e.g., heterostructures by growing a magnetic layer on a Rashba superconductor [67], superconducting doped topological insulator [68–70], etc. However, here we would not like to make any direct connection between our theoretical toy model and promising candidate material and relevant experiments. We rather investigate the effect of various magnetic textures in the form of in-plane and out-of-plane Néel-type, Bloch-type, etc., spin spirals (SSs) on the topological superconducting phase. Depending on the spin configuration of the magnetic impurities, we observe a phase transition from TSC to trivial superconductor. As a result, the MZMs disappear via a gap closing within the Shiba bands. The system periodically returns back to the original TSC phase as the spins rotate back to their initial configuration. Considering a lattice model, we also show that the Majorana peak height in the local density of states (LDOS) gradually becomes smaller in magnitude as we rotate the spin configuration and eventually vanishes in the trivial phase. This also becomes evident from similar analysis in our 2D model. Initially, the MZMs can hybridize with the Majorana edge modes (MEMs) present for a pure 2D *p*-wave superconducting substrate, i.e., in the absence of any magnetic spin chain. Such MEMs disappear at some critical value of the chemical potential and exchange coupling strength and, hence, only the MZMs survive within the Shiba bands. These MZMs are further destroyed as we tune the spin configuration of the magnetic impurities. We further analytically emphasize that the spin configuration of the magnetic impurities induces an effective *s*-wave pairing in the nontrivial phase of the magnetic chain, resulting in a phase transition between topologically nontrivial to trivial superconductors.

The remainder of the paper is organized as follows. In Sec. II, we present our 1D lattice model including various possible configurations of the impurity spin chains. We discuss our numerical results for the band spectrum, LDOS, topological invariant, and analytical results for the effective pairing gap in Sec. III. In Sec. IV, we discuss our 2D results based on a lattice model. Finally, we summarize and conclude our paper in Sec. V.

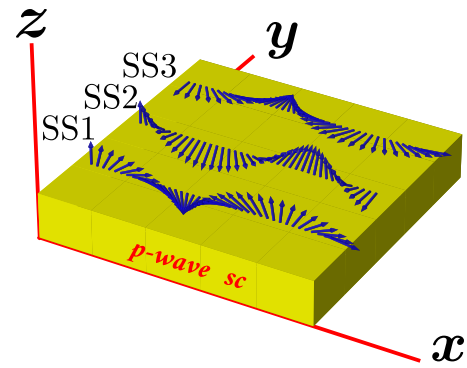

FIG. 1. Schematic setup of our model where different 1D SSs, representing chain of magnetic impurities, are placed on a *p*-wave superconductor. Different spiral textures are schematically depicted by the SSs with propagation vector along the *x* axis with different rotational axes as (SS1) out-of-plane Néel-type, (SS2) Bloch-type, and (SS3) in-plane Néel-type impurity spin chains.

II. MODEL HAMILTONIAN AND IMPURITY SPIN TEXTURE

In this section we construct a 1D tight-binding lattice model considering different orientations of the impurity spin chains and our supporting observable.

A. Tight-binding model and different impurity spin configurations

We consider a 1D chain of magnetic impurities placed on a superconducting substrate essentially with *p*-wave (spin-triplet) pairing. Our setup is schematically shown in Fig. 1. We can effectively describe this system using a 1D lattice model with the following Hamiltonian:

$$H = \sum_{l,\alpha}(t_l c^{\dagger}_{l,\alpha} c_{l+1,\alpha} + \text{H.c.}) - \mu \sum_{l,\alpha} c^{\dagger}_{l,\alpha} c_{l,\alpha} + \sum_{l,\alpha,\beta} (\vec{B}_l \cdot \vec{\sigma})_{\alpha,\beta} c^{\dagger}_{l,\alpha} c_{l,\beta} + \Delta_p \sum_{l,\alpha} (c^{\dagger}_{l,\alpha} c^{\dagger}_{l+1,\alpha} + \text{H.c.}), \tag{1}$$

where $c^{\dagger}$ and c correspond to electron creation and annihilation operators, respectively, for the superconductors, t is the electron hopping amplitude between adjacent spins in the 1D chain, μ is the chemical potential, and Δ_p is the spin-symmetric triplet order parameter of the superconductor [61,71]. The doping of electron or hole depends on the sign of μ. Here, we assume $t_l = t_l^* = t$ and set $t = 1$ for the overall energy scale of our system. The third term represents the exchange coupling between the magnetic impurity spin and the electron spin of the superconductor. We assume that all magnetic impurity spins in the chain are classical spins and each spin is represented by a three-dimensional vector

with a magnitude S. This assumption only remains valid for large S were the quantum fluctuations of impurity spins can be neglected. Hence, the impurity spins interacting with the electronic spin $\vec{\sigma}$ can be replaced by an effective local magnetic field as $\vec{B}_l = B_0\hat{S}_l$ in our model, where $B_0 = JS$, J is the magnetic exchange coupling strength, $\hat{S}_l$ is the site-dependent impurity spin direction. Also, l and α, β correspond to the lattice sites and spin indices, respectively. Then one can write the unit vector along impurity spin direction in spherical polar coordinate system [35,36] as

$$\hat{S}_l = \sin\theta_l \cos\phi_l \hat{i} + \sin\theta_l \sin\phi_l \hat{j} + \cos\theta_l \hat{k}, \tag{2}$$

where $\theta_l = G_s x_l$ [72] and $\phi_l = G_h x_l$ [73], $x_l = la$, a is the lattice constant which has been considered to be unity. Note that θ (cone angle) and ϕ are two important quantities to determine the noncollinear spiral configuration. For a fixed value of ϕ_l (θ_l), G_s (G_h) determines the period of SS. In our model, the impurity spin chain propagates along the x direction as shown in Fig. 1. There are a number of cases that arise depending on different configurations of the inpurity spins [37] and a few cases are mentioned below.

(1) When $\phi_l = 0$ and $\theta_l = G_s x_l$, then the impurity spin rotates in the xz plane as shown in Fig. 1, named SS1. Therefore, spin rotation axis lies perpendicular to the direction of propagation of the SS. This is called out-of-plane Néel-type SS configuration [74].

(2) On the other hand, spiral configuration with $\phi_l = \pi/2$ and $\theta_l = G_s x_l$ corresponds to rotation axis of impurity spins parallel to the direction of propagation, i.e., in the yz plane [38,39,75]. Such configuration with helical modulation is called Bloch-type SS configuration, named SS2 in Fig. 1.

(3) Now, if θ_l, the cone angle is fixed to $\pi/2$ and $\phi_l = G_h x_l$, inpurity spins rotate in the xy plane with rotational axis perpendicular the x axis. Such configuration is known as in-plane Néel-type SS, named SS3 in Fig. 1. This type of SS configuration is also commonly known as flat spiral. Additionally, for $0 < \theta_l < \pi/2$ and $\phi_l = G_h x_l$, the spiral structure takes the conical SS form.

(4) One can in general consider the situation where both θ_l and ϕ_l change with respect to the lattice site index l, resulting in a complex spin texture [see Fig. 2(b) as a schematic example].

In our analysis, we mainly focus on cases 1 and 4 throughout the paper. After transforming to the Bogoliubov basis $\Phi_l = (c_{l,\uparrow}, c_{l,\downarrow}, c^\dagger_{l,\downarrow}, -c^\dagger_{l,\uparrow})$, the Hamiltonian in Eq. (1) takes the form

$$H = \sum_l (\Phi_l^\dagger \tilde{\mathcal{T}}_l \Phi_{l+1} + \text{H.c.}) + \Phi_l^\dagger \tilde{\mathcal{E}}_l \Phi_l, \tag{3}$$

where the matrices $\tilde{\mathcal{T}}_l$ and $\tilde{\mathcal{E}}_l$ can be written as

$$\tilde{\mathcal{T}}_l = \begin{pmatrix} t & 0 & 0 & -\Delta_p \\ 0 & t & \Delta_p & 0 \\ 0 & -\Delta_p & -t & 0 \\ \Delta_p & 0 & 0 & -t \end{pmatrix}, \tag{4}$$

$$\tilde{\mathcal{E}}_l = \begin{pmatrix} -\mu\sigma_0 + \vec{B}_l.\vec{\sigma} & O_{2\times2} \\ O_{2\times2} & \mu\sigma_0 + \vec{B}_l.\vec{\sigma} \end{pmatrix}. \tag{5}$$

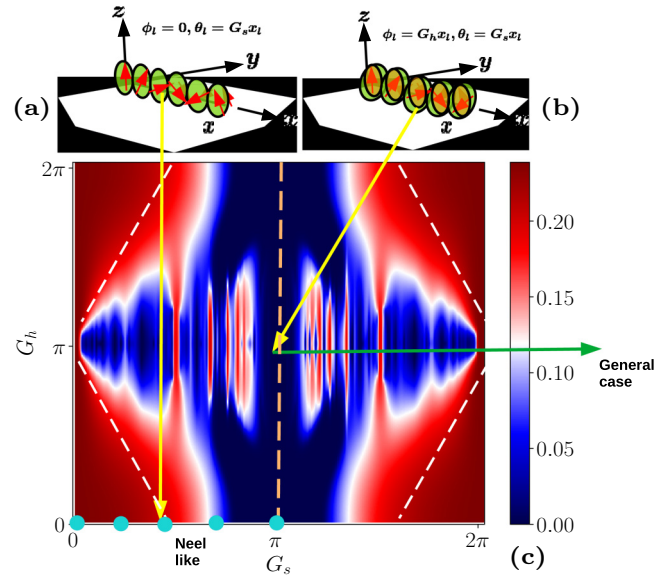

FIG. 2. (a) Spin-chain configuration for the Néel-type rotation in the xz plane for $G_h = 0$. (b) Spin-chain configuration for the general type of rotation on a sphere, where both $G_s, G_h \neq 0$. (c) Numerical results for LDOS peak height at $E = 0$ are shown in the $G_s - G_h$ plane. The color bar at the right most indicates the amplitude of LDOS peak in an arbitrary unit. Here, we choose the other model parameters as $\mu = 4t$, $B_0 = 5t$, $\Delta_p = t$.

Here, σ_0 and $\vec{\sigma} = (\sigma_x, \sigma_y, \sigma_z)$ are 2×2 identity matrix and Pauli matrices in spin space, respectively, and $O_{2\times2}$ is a null matrix. Index l runs from 0 to N (any finite number of lattice sites). We consider $N = 48$ throughout our numerical computation employing open boundary condition (OBC).

B. Observable

To understand the physical presence of MZMs in a real system, one needs to calculate the LDOS [35,66]. This identifies the topological superconducting phase by manifesting a zero-bias peak (ZBP) associated with the MZMs at the end of the impurity spin chain, whereas the middle of the system exhibits the presence of Shiba bands within the superconducting gap [35,66]. The energy difference between the two Shiba bands' main peaks (on either side of the Majorana ZBP) can be defined as a band gap, called "minigap" Δ_m [35]. Sign change of this minigap corresponds to nontopological to topological phase transition [35,38]. The quasiparticle LDOS for the ith site and at a given energy E can be defined as [35,40]

$$D_i(E) = \sum_{n\sigma} \left(|u^n_{i\sigma}|^2 + |v^n_{i\sigma}|^2\right)\delta(E - E_n), \tag{6}$$

where $u^n_{i\sigma}$ and $v^n_{i\sigma}$ are the electronlike and holelike quasiparticle amplitudes, respectively. Here, n and σ being the eigenvalue and spin indices, respectively.

III. RESULTS

In this section, we discuss our numerical results based on the lattice model as well as the analytical treatment by considering a continuum model to support the former. We mainly

focus on the discussions of how the topological properties of the system, in particular, the MZMs in the TSC phase, are gradually destroyed due to the effect of different SS configurations, captured in their LDOS behavior. This essentially establishes that the p-wave superconducting gap contribution gradually decreases and the s-wave pairing gap amplitude grows with the controlled modulation of G_h and G_s in spin chains.

A. LDOS at $E = 0$ in $G_s - G_h$ plane

In this subsection, we discuss the results of our model mainly for a general case where a chain of magnetic impurities along the x direction is engineered via controlled variations of G_s and G_h on top of a p-wave superconducting substrate. Due to the freedom of choosing different rotational configurations of impurity spins on the surface of a sphere, governed by G_s, G_h values, interesting phenomena can occur on the Majorana ZBP and the corresponding topological phase. In Fig. 2, we summarize our results in the $G_s - G_h$ plane. Figure 2(a) illustrates the schematic of a special case of SS with the rotation axis perpendicular to the xz plane. Hence, along the $G_h = 0$ line ($\phi_l = 0$), the linearly varying θ_l with lattice sites keeps Néel-type spin rotation with a period $\frac{2\pi}{G_s}$ in the unit of lattice constant. Furthermore, Fig. 2(b) schematically represents the more general case of a SS configuration with an arbitrary rotational axis direction due to both $G_s, G_h \neq 0$, i.e., both θ_l and ϕ_l vary linearly with the lattice sites. In Fig. 2(c), we show the variation of zero-energy LDOS as a function of G_s and G_h such that both θ_l and ϕ_l vary with the 1D lattice sites. Here, LDOS is computed employing the formula mentioned in Eq. (6). Also, this LDOS is presented corresponding to the end of the finite chain where MZMs are present in the topological regime. At the four corner points in Fig. 2(c) corresponding to $G_s, G_h = (0, 0), (0, 2\pi), (2\pi, 0)$, and $(2\pi, 2\pi)$, the alignment of all spins is ferromagnetic in the chain. Those corner points and their nearby regime indicate Kitaev chains [19,60] with pure spin-symmetric triplet p-wave pairing gap Δ_p, highlighted by maroon color regime within the dashed white line in Fig. 2(c). The LDOS at zero energy becomes maximum at those points, indicating topological superconducting phase hosting MZMs at the ends of the chain. Additionally, the red region beyond the white dashed line in Fig. 2(c) where the noncollinear spin configurations are determined by $G_s, G_h \neq 0$, the p-wave pairing is significantly strong enough to host MZMs which, however, gradually disappear in the blue region. This is due to the fact that an effective s-wave pairing is generated, giving rise to a trivial phase in the deep blue region. As a result, the LDOS peak height at $E = 0$ decreases significantly to a small value from its maximum value of about 0.25 (in arbitrary unit [35]). Therefore, the thin white regime separating red and blue regions in Fig. 2(c) represents roughly the phase boundary between topologically nontrivial and trivial superconducting phases via a nontrivial gap closing. Note that, when it enters into the topologically trivial phase, the zero-energy LDOS peak height becomes vanishingly small and a trivial s-wave gap opens along $G_s = \pi$ line, as indicated by a vertical dashed line at the middle of Fig. 2(c). In this regime, no MZMs are present as the p-wave pairing contribution is destroyed and the system hosts an effective s-wave pairing (see further discussion on this effective s-wave contribution in the subsequent subsections).

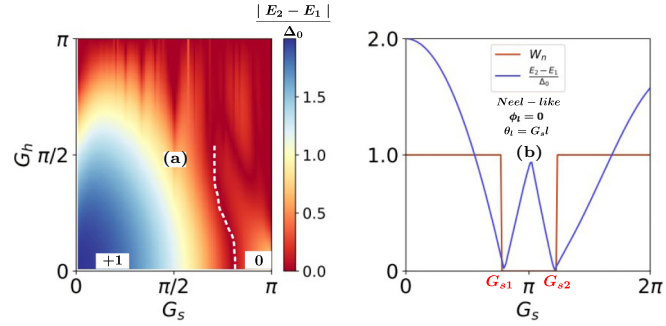

FIG. 3. (a) Band gap ($E_2 - E_1$) (normalized by Δ_0) is shown as a function of two spiral wave vectors G_s and G_h considering purely p-wave pairing. Here, we choose $\mu = 4t, B_0 = 5t$. (b) Winding number W_n is depicted as a function of G_s for the Néel-type ($\phi_l = 0$) rotation of the magnetic impurities. The gap closing points and the concomitant jumps of W_n indicate the topological phase transition.

B. Topological characterization

From the features of LDOS, one can only observe how the Majorana peak height gradually decreases as we tune the spiral wave-vector configuration. In this regard, we illustrate the variation of gap structure $|E_2 - E_1|/\Delta_0$ in $G_s - G_h$ plane where the maroon lines (one such marked by the dashed white line for guide to the eye) indicate the boundary region between topologically nontrivial ($W_n = +1$) and trivial ($W_n = 0$) phases [see Fig. 3(a)]. It has been clearly shown that when $G_h = 0$, gap closing takes place around $G_s \sim 2.5$. In order to characterize the topological phase of our model, we also calculate the topological invariant considering the Néel-type SS configuration. As our lattice model does not satisfy translation symmetry, but continues to preserve the chiral symmetry in the presence of the magnetic impurities, we follow Refs. [76,77] to compute the winding number W_n in real space. The corresponding winding number W_n is shown for the case when $\phi_l = 0$ and $\theta_l = G_s l a$ (Néel type as shown in Fig. 1) in Fig. 3(b). It is evident that there are sharp topological phase transitions around $G_{s1} = 2.5$ and $G_{s2} = 3.7$ where W_n jumps from $1 \to 0$ in accordance with the gap $|E_2 - E_1|$ closing points. This also matches with the $G_h = 0$ line of Fig. 3(a). The topological superconducting phase with $W_n = +1$ hosts Majorana zero modes. This gives a clear signature of the topological phase transition in our model. Furthermore, for the Néel-type rotation, an analytical understanding of the gap structure is presented in Appendix C.

C. Detailed study of the topologically nontrivial to trivial superconductor phase transition for Néel-type rotation in the magnetic impurity chain

In this subsection, we further discuss the outcome for a Néel-type rotation of impurity spin chain, SS1 depicted in Fig. 1. In this case, we obtain the variation of different physical quantities for a SS with varying period by changing

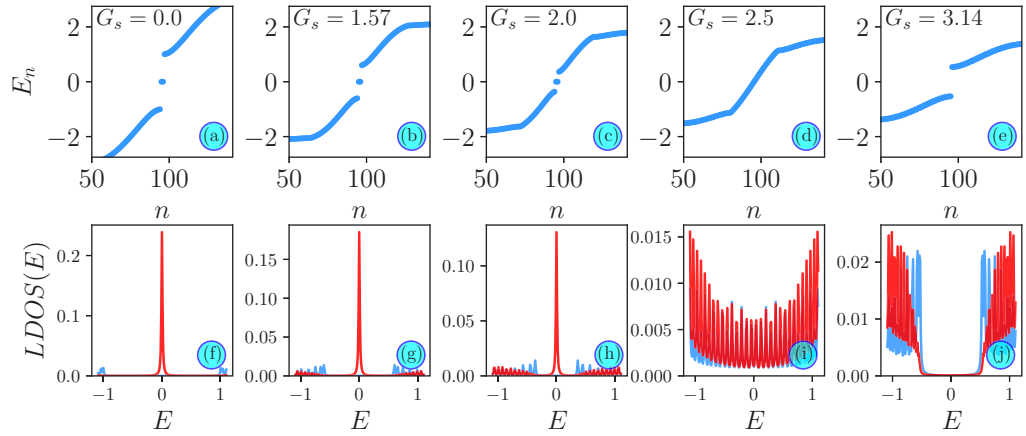

FIG. 4. (i) The first row, (a)–(e), represents the eigenvalue spectrum for a finite-size 1D chain considering different values of spiral wave vector $G_s = 0.0, 1.57, 2.0, 2.5, 3.14$. Here, we choose the other model parameters as $\mu = 4t$, $B_0 = 5t$, $\Delta_p = t$. (ii) In the second row, (f)–(j), we show the LDOS as a function of energy for the same set of SS wave vector G_s and choosing the same parameter values as mentioned above. The Majorana ZBP is indicated by the red plots in (f)–(h) when LDOS is computed at the end of the finite chain, whereas blue plots denote the Shiba bands in LDOS when they are measured at the middle of the chain.

G_s while keeping $\phi_l = 0$. In Figs. 4(a)–(e), we show the eigenvalue spectrum for different values of G_s, considering a finite-size system with OBC. Those G_s values are approximately marked by the cyan dots on the G_s axis of Fig. 2(c). This enables one to understand the appearance and disappearance of MZMs under the influence of SS period. For $G_s = 0$ and 2π, a pair of MZMs appears at the two ends of a finite chain due to pure p-wave superconductivity, i.e., the Kitaev limit [19,59–61]. Around these points, MZMs appear with the condition $B_0 \geqslant \sqrt{\mu^2 + \Delta_p^2}$ [27,28], akin to the 1D nanowire case. Due to the modulation of SS wave vector by changing G_s, the topological superconducting gap or the minigap Δ_m within the Shiba bands gradually decreases and the MZMs lying in the gap disappear from the system for $G_s = 2.45$. Interestingly, a nontrivial gap closing takes place within the Shiba bands for a particular period of the SS corresponding to $G_s = 2.45$ as shown in Fig. 4(d). However, further modulation of G_s up to π opens up a trivial superconducting gap without MZMs in the system. The $G_s = \pi$ represents an antiferromagnetic spin-chain configuration and with further rotation of spins from π, the spin chain will again become a ferromagnetic chain at $G_s = 2\pi$ point. Therefore, within $2\pi > G_s > \pi$, the phenomena repeat as we move away from 2π point towards π point and the Kitaev phase reappears at $G_s = 2\pi$.

The main underlying physics of our model is governed by the modulated spin textures which can be characterized by G_h and G_s. Here, it is worth to mention that noncollinear magnetism [75,78] including spin-spiral order [74] occurs due to the competition between underlying Heisenberg exchange interaction and the Dzyaloshinskii-Moriya (DM) interaction. In most cases where magnetic layer or chain is grown on metallic or semiconducting substrate, the ubiquitous Ruderman-Kittel-Kasuya-Yosida (RKKY) exchange tensor between magnetic atoms contains both Heisenberg exchange and DM interactions. The antisymmetric DM interaction is the result of spin-orbit coupling that occurs in magnetic heterostructures due to the broken inversion symmetry. In addition, there may exist another spin-orbit coupling induced interaction parameter called axial magnetic anisotropy constant. In order to engineer G, one needs to have control on these interaction parameters. Indeed, these parameters are highly tunable through intercalation [79], electron doping [78], thickness [80], and adjusting the interatomic distances [83], etc. Hence, the smooth variation in G can be attributed to the high tunability of RKKY exchange tensor and magnetocrystalline anisotropy energy.

In the presence of superconducting substrate, the exchange frustration arises from the similar RKKY-type exchange interactions between the impurity spins [38,41,84]. Such RKKY-type interaction between two magnetic impurities at a distance x_{ij} apart can be mediated via the virtual exchange of electron-hole excitations whereas superconductivity prohibits the pairs with energy less than the superconducting gap. As a result, system exhibits an effective pairing gap which depends on x_{ij} and spin spiral wave vector. Hence, for our case, the physical reason behind the disappearance of zero-energy MZMs can be attributed to the fact that interplay of Néel-type spin spiral order and p-wave superconductivity generates an effective pairing gap which is s wave in nature. This can be written in real space as

$$\tilde{\Delta}_{ij}^{\text{eff}} = -(\epsilon_0/2)\delta_{ij} - (1-\delta_{ij}) \times \left[\frac{\Delta_t}{\sqrt{1+\tilde{\Delta}_p^2}} \sin(k_F'|x_{ij}|) + \gamma \Delta_t \cos(k_F' x_{ij})\right] \times e^{-\frac{|x_{ij}|}{\xi_0}} \cos\left(\frac{G_s}{2} x_{ij}\right), \tag{7}$$

where $x_{ij} = x_i - x_j$, $k_F' = \frac{k_F}{\sqrt{1+\tilde{\Delta}_p^2}}$, $\tilde{\Delta}_p = \Delta_p/V_F$, $\Delta_t = \frac{\Delta_p k_F}{\sqrt{1+\tilde{\Delta}_p^2}}$, and $\gamma = \frac{\tilde{\Delta}_p}{\sqrt{1+\tilde{\Delta}_p^2}}$.

Here, $\xi_0 = V_F/\omega(0)$ is the superconducting coherence length, V_F and k_F are the Fermi velocity and Fermi momentum, respectively, and $\omega(0) = \Delta_t/\sqrt{1+\tilde{\Delta}_p^2}$. ϵ_0 is the YSR

bound-state energy in the deep Shiba limit when a single magnetic impurity is placed on a p-wave superconductor [85]. Detailed analytical derivation of Eq. (7) is presented in Appendix B based on a low-energy continuum model. It is evident from Eq. (7) that the nature of the effective gap is s-wave like as $\tilde{\Delta}_{ij}^{\text{eff}} = \tilde{\Delta}_{ji}^{\text{eff}}$. Due to the emergence of effective s-wave pairing, the system approaches to a trivial superconducting phase with the modulation of G_s within the range $\pi \gtrsim G_s \gtrsim 2.5$. Particularly at $G_s = \pi$, the SS corresponds to the antiferromagnetic spin chain and the effective gap is purely s-wave type, consistent with the earlier reports [73].

To elaborate further, in Figs. 4(f)–(j), we discuss about the variation of LDOSs as a function of energy with different values of G_s. In the topological regime, if we compute the LDOS at the end of the finite chain, we obtain Majorana ZBP (red color) at exactly zero energy ($E = 0$). On the other hand, the feature of LDOS at the middle of the chain indicates nontopological Shiba band (blue color) within the superconducting gap $-\Delta_p$ to Δ_p [35,66]. Distance between the two closest Shiba peaks on either sides of the $E = 0$ peak is called the minigap Δ_m [35]. From Fig. 4(f), it is evident that the height of the Majorana ZBP for $G_s = 0$ is maximum, $\approx$0.25 in an arbitrary unit. Concomitantly, no Shiba peak appears within $-\Delta_p$ to Δ_p as the impurities are ferromagnetically aligned. Height of the Majorana peak at $E = 0$ decreases with the enhancement of G_s. Eventually, at $G_s = 2.5$, Majorana ZBP disappears and it refers to a gapless phase in LDOS. Finally, we obtain some trivial gap in LDOS spectrum at $G_s = \pi$. Simultaneously, the signature of Shiba bands is reflected in the LDOS behavior within $-\Delta_p$ to Δ_p [see Figs. 4(g)–(j)] when $G_s \neq 0$. This can be understood as we increase G_s, the magnitude of minigap Δ_m decreases with G_s, and at $G_s = 2.45$, it vanishes. Afterwards, further increase of G_s enables the minigap to change sign and $|\Delta_m|$ increases further in magnitude. Sign change of minigap (Δ_m) indicates the topological to nontopological phase transition.

In Fig. 5, we explain the variations of important physical quantities as a function of G_s for out-of-plane Néel-type SSs. In Fig. 5(a), we depict the variations of the energy spectrum within the range $-\Delta_p$ to Δ_p, as a function of G_s. The spectrum exhibits 2π periodicity with respect to G_s. For $G_s = 0$, the system is in the Kitaev limit manifesting topological superconducting phase and thus we always obtain the MZMs, indicated by the red line in Fig. 5(a). Majorana modes merge into the bulk states and disappear completely around $G_s = 2.5$ as after that the system purely behaves like a trivial s-wave superconductor. Interestingly, we observe that Shiba bands within $-\Delta_p$ to Δ_p (precisely, above $|E/\Delta_p| \gtrsim 0.6$) in the trivial s-wave superconducting phase oscillate as they interfere with each other in the presence of a magnetic impurity chain. This can be clearly visible in Fig. 5(b) where the interference of Shiba bands exhibits oscillations around $G_s = \pi$ SS configuration, within a range $3.8 \gtrsim G_s \gtrsim 2.5$. Such type of oscillations can be another evidence of the formation of an effective pure s-wave pairing and is absent in the nontrivial topological p-wave superconducting phase. In Appendix A, we discuss in detail that similar oscillations of Shiba bands can be obtained when 1D spin spiral is placed on a purely s-wave superconductor. With further increase in G_s beyond $G_s \approx 3.8$ value, the system starts to tune itself and the initial

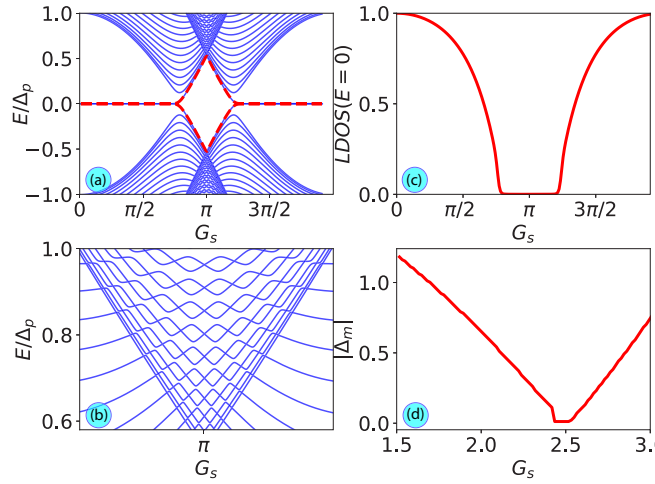

FIG. 5. (a) Band spectrum where the energy E is plotted as a function of G_s within the energy range $-\Delta_p$ to Δ_p. (b) Enlarged view of the energy spectrum is shown as a function of G_s, around the trivial gapped region in the vicinity of $G_s = \pi$. (c) LDOS at $E = 0$ is shown as a function of G_s and the vanishing LDOS represents the trivial s-wave gapped phase. (d) Variation of the absolute value of the minigap (Δ_m) is illustrated as a function of G_s. Here, other model parameters are chosen as $\mu = 4t$, $B_0 = 5t$, $\Delta_p = 1.0t$.

topological superconducting phase with a dominant p-wave pairing reappears as shown by the normalized LDOS peak height behavior with change of G_s in Fig. 5(c). The Majorana ZBP height is maximum for the ferromagnetic spin chain corresponding to $G_s = 0$ and 2π. As we tune the G_s towards π, a smooth variation of the Majorana peak height is observed as a function of G_s. Interestingly, it monotonically decreases up to $G_s \approx 2.5$ ($G_s \approx 3.8$) starting from $G_s \approx 0$ ($G_s \approx 2\pi$) and after that the Majorana peak disappears. The corresponding gap in the LDOS signifies emergence of topologically trivial phase with an effective s-wave pairing. Therefore, in a real system, one can control the appearance and disappearance of MZMs using the variation of SS wave vector. In Fig. 5(d), we depict the variation of the absolute value of the minigap (Δ_m) as a function of the G_s. The absolute value of Δ_m gradually decreases from its maximum value at $G_s = 0$ and vanishes around $G_s = 2.5$, referring to the topological phase in the system. A small plateau corresponding to $\Delta_m = 0$ indicates a gapless phase near $G_s = 2.5$ [see also Figs. 4(d) and 4(i)] and afterwards its magnitude rises again as one changes G_s. Hence, it is evident that there is a sign change of Δ_m within the Shiba bands, indicating a topological phase transition from a nontrivial p-wave to a trivial s-wave superconductor through a gapless phase.

D. Analytical results based on continuum model

In this subsection, we discuss our analytical approach for the Néel-type rotation in order to support our numerical results presented in the previous subsection. Our analytical calculation is based on an effective continuum theory of our lattice model in Eq. (1). A similar approach was reported earlier in case of a chain of magnetic impurities placed on an s-wave superconductor [38,42,43]. From the features of the energy

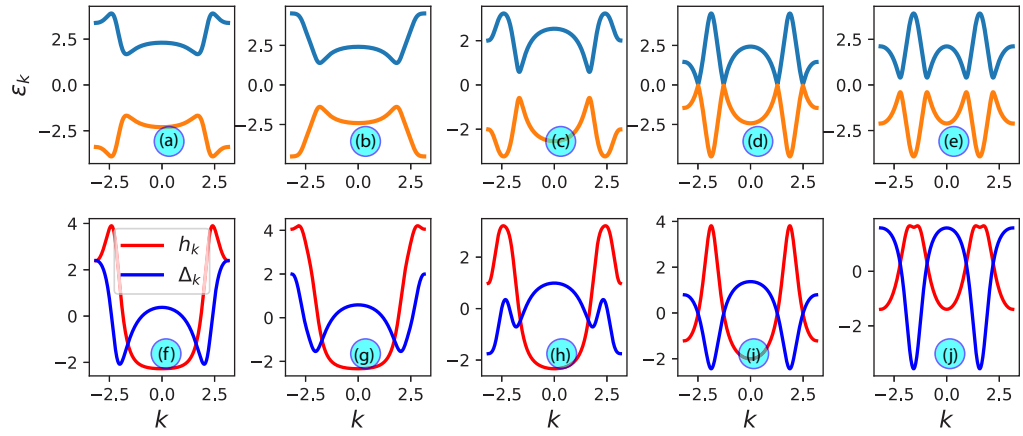

FIG. 6. (i) In the first row, (a)–(e), we show the behavior of the energy eigenvalue spectrum ϵ_k for five different values of $G_s = 0.0, 1.57, 2.0, 2.55, 3.14$. (ii) Second row, (f)–(j), represents the variation of the onsite term h_k and the effective pairing gap Δ_k as a function of the propagating vector k, considering the same set of G_s values as mentioned above. Here, we choose the other parameters as $\epsilon_0 = 0$, $\xi_0 = 2a$, $k_F a = (2\pi + G_s/2)$.

spectrum, the effective gap structure and total density of states (DOS) presented in Figs. 6 and 7, respectively, we confirm the topological phase transition along with the nature of an effective s-wave pairing gap.

We begin from the low-energy continuum model [Bogoliubov–de Gennes Hamiltonian (BdG)] in which a 1D chain of localized magnetic impurities is placed on a p-wave superconductor,

$$H = \xi_k \tau_z - J \sum_j (\vec{S}_j \cdot \vec{\sigma}) \delta(x - x_j) + \Delta_p k \tau_y, \tag{8}$$

where $\xi_k = \frac{k^2}{2m} - \mu$, k is the wave vector corresponding to a model with 1D spin chain placed on a superconducting substrate with pairing gap Δ_p. Particle-hole and spin degrees of freedom can be expressed in terms of the Pauli matrices

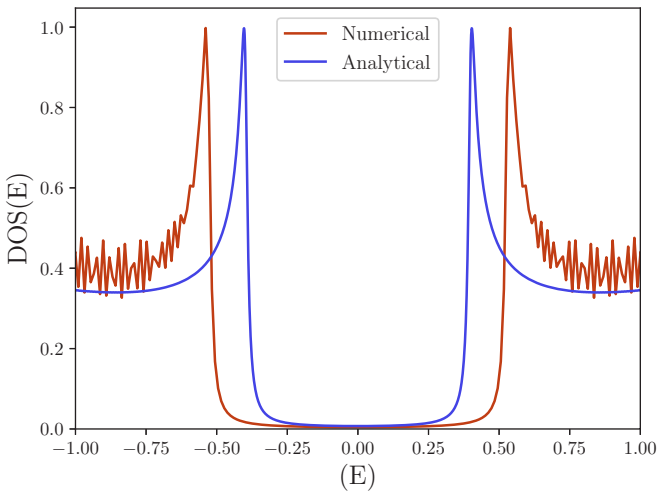

FIG. 7. Normalized total DOS is shown as a function of energy E for $G_s = \pi$, i.e., when impurity spins follow antiferromagnetic alignment. Here, numerical and analytical results are indicated by red and blue colors, respectively. We choose the other model parameters as $\mu = 4t$, $B_0 = 5t$, $\Delta_p = 1.0t$ and $\epsilon_0 = 0$, $\xi_0 = 2a$, $k_F a = (2\pi + G_s/2)$ for our numerical and analytical computation, respectively.

τ and σ, respectively. Starting from this model one can obtain an effective pairing gap in real space as mentioned in Eq. (7). The calculational details are presented in Appendix B. Hence, taking Fourier transform of this effective gap and diagonal components of the real-space Hamiltonian, we obtain diagonal elements (h_k) and effective pairing gap (Δ_k) as nondiagonal elements in momentum space. The analytical expressions of h_k and Δ_k for our 1D chain can be written as

$$h_k = \frac{\epsilon_0}{2} - \frac{1}{2}\Bigg\{k'_F \Delta_p \Bigg[F_1\left(k + \frac{G_s}{2}\right) + F_1\left(k - \frac{G_s}{2}\right)\Bigg] + \gamma \Delta_t \Bigg[F_2\left(k + \frac{G_s}{2}\right) + F_2\left(k - \frac{G_s}{2}\right)\Bigg]\Bigg\}, \tag{9}$$

$$\Delta_k = -\frac{\epsilon_0}{2} + \frac{1}{2}\Bigg\{\frac{\Delta_t}{\sqrt{1 + \tilde{\Delta}_p^2}} \Bigg[F_4\left(k + \frac{G_s}{2}\right) + F_4\left(k - \frac{G_s}{2}\right)\Bigg] + \gamma \Delta_t \Bigg[F_3\left(k + \frac{G_s}{2}\right) + F_3\left(k - \frac{G_s}{2}\right)\Bigg]\Bigg\}. \tag{10}$$

Therefore, from the BdG Hamiltonian (see Appendix B for details) we can obtain the effective energy spectrum of our system as $\epsilon_k = \pm\sqrt{h_k^2 + \Delta_k^2}$. In Eqs. (9) and (10), $\epsilon_0 = 2\Delta_t/\alpha$ is the Shiba bound-state energy for a single magnetic impurity placed on a p-wave superconductor [85], $\alpha = JS/(V_F\sqrt{1 + \tilde{\Delta}_p^2})$ is the impurity strength, and the renormalized Fermi momentum $k'_F = k_F/\sqrt{1 + \tilde{\Delta}_p^2}$. The corresponding functions which we have defined in Eqs. (9) and (10) read as

$$F_1(k) = \mathrm{Im}\left[\frac{i}{1 - e^{\frac{a}{\xi_0} - i(k'_F + k)}} + \frac{i}{1 - e^{\frac{a}{\xi_0} - i(k'_F - k)}}\right], \tag{11}$$

$$F_2(k) = \mathrm{Re}\left[\frac{i}{1 - e^{\frac{a}{\xi_0} - i(k'_F + k)}} + \frac{i}{1 - e^{\frac{a}{\xi_0} - i(k'_F - k)}}\right], \tag{12}$$

$$F_3(k) = \mathrm{Re}\left[\frac{1}{1 - e^{\frac{a}{\xi_0} - i(k'_F + k)}} + \frac{1}{1 - e^{\frac{a}{\xi_0} - i(k'_F - k)}}\right], \tag{13}$$

$$F_4(k) = \mathrm{Im}\left[\frac{1}{1 - e^{\frac{a}{\xi_0} - i(k'_F + k)}} + \frac{1}{1 - e^{\frac{a}{\xi_0} - i(k'_F - k)}}\right], \tag{14}$$

where ξ_0 is the superconducting coherence length. In principle, in our model Hamiltonian [Eq. (1)], we always consider $\xi_0 \to \infty$ limit so that mean field theory of superconductivity remains valid [86]. Therefore, in the theoretical model [Eq. (8)] we always consider $\xi_0 > a$ throughout our analysis.

In Figs. 6(a)–(e), we depict the variation of the energy spectrum ϵ_k for Néel-type rotation of the magnetic impurities, choosing different values of G_s. Moreover, Figs. 6(f)–(j) represent the variation of both the effective gap Δ_k and h_k as a function of k, employing Eqs. (9) and (10), respectively. For $G_s = 0$ case, the superconducting gap is p wave in nature. Therefore, we obtain a topologically nontrivial gap in the energy spectrum [see Fig. 6(a)]. This phase hosts MZMs. Afterwards, this gap became smaller in magnitude with increasing G_s, as one compares the gap around $\epsilon_k = 0$ in Figs. 6(b) and 6(c). Eventually, this gap closes at $G_s = 2.55$ and after that it again open up as evident from Figs. 6(d) and 6(e). Therefore, a topological phase transition takes place at $G_s = 2.55$. This phenomenon can also be understood from the individual behavior of Δ_k and h_k for the same set of G_s values. Most importantly, this gap closing and reopening phenomenon within our analytical treatment matches with our numerical results where it has been shown to take place at slightly lower value of G_s, which is 2.5.

For $G_s = \pi$, when impurity spins form an antiferromagnetic spin chain, the gap in the energy spectrum is trivial [see Fig. 6(e)]. However, this gap is not insulating as evident from the variation of Δ_k at $G_s = \pi$ in Fig. 6(j). Hence, one can conclude that it should be a trivial superconducting phase rather than a trivial insulator. To confirm that this superconducting phase is effectively s wave in nature, we compute the total DOS, both numerically as well as analytically, and compare their behavior at $G_s = \pi$ as a function of energy as shown in Fig. 7. We employ the following formula to numerically compute the total DOS as

$$D(E) = \frac{1}{\pi} \sum_n \delta(E - E_n), \tag{15}$$

where the sum is taken over the energy eigenvalues (E_n) of Eq. (1) and $\delta(E - E_n)$ is modeled using a Lorentzian with broadening $0.01t$. Analytically, normalized total DOS can be calculated from the formula

$$D(E) = \int_{-\pi}^{\pi} \frac{dk}{2\pi} \delta(E - \epsilon_k), \tag{16}$$

where $\epsilon_k = \pm\sqrt{h_k^2 + \Delta_k^2}$ and we use Eqs. (9) and (10). Note, we obtain qualitatively similar features of total DOS for both the cases at $G_s = \pi$. In particular, quasiparticle peaks appear at $\Delta_{\text{eff}} \simeq \Delta_p/2$ and after that they decay as can be seen from Fig. 7. Hence, we conclude that this superconducting phase is conventional s-wave like with no MZMs present.

IV. DISCUSSION CONSIDERING 2D *p*-WAVE SUPERCONDUCTOR

In this section, we consider a 1D magnetic spin chain (locally varying) on top of a 2D p-wave superconductor. We can describe this 2D system using the following Hamiltonian as

$$H_{\text{2D}} = \sum_{l,\alpha} (t_l c^\dagger_{l,\alpha} c_{l+1,\alpha} + \text{H.c.}) - \mu \sum_{l,\alpha} c^\dagger_{l,\alpha} c_{l,\alpha} + \sum_{l,\alpha,\beta} (\vec{B}_l \cdot \vec{\sigma})_{\alpha,\beta} c^\dagger_{l,\alpha} c_{l,\beta} + \Delta_p \sum_{l,\alpha} (c^\dagger_{l,\alpha} c^\dagger_{l+1,\alpha} + \text{H.c.}). \tag{17}$$

Here, the index l accounts for the x and y coordinates of the corresponding 2D lattice sites. In particular, we choose $l = (n, m)$ in 2D, and the number of sites along x (y) direction is N_x (N_y). Other symbols in Eq. (17) indicate the same meaning as mentioned after Eq. (1). A pure 2D p-wave superconductor (in absence of any magnetic spin chain) exhibits a gapless topological superconducting phase at the bulk of the system hosting MEMs of flat type [87,88]. Afterwards, we incorporate a 1D magnetic spin chain on top of this 2D p-wave superconductor. Here, the ends of the chain lie exactly on the edge of the superconducting substrate. Initially, for some specific values of the exchange coupling strength ($B_0 = JS$) and chemical potential (μ) of the system (when the chain is in the topological regime), MZMs (localized at the two ends of the magnetic chain) can hybridize with the MEMs. Hence, one cannot distinguish between the MEMs and MZMs in this regime. However, MEMs disappear at some specific values of the μ and B_0 even when the chain is in the topological regime. Only MZMs can survive and they are localized at the two ends of the chain. In this case, the Shiba states are energetically separated from the rest of the system. This is the prime reason for the suppression of the hybridization of the MZMs with the MEMs. Hence, this feature hints towards an interesting interplay between μ and B_0, which makes the distinction between MEMs and MZMs possible when the chain is in the topological regime. However, it is difficult to find an analytical condition between μ and B_0 in the case of a 2D p-wave superconductor in presence of the magnetic spin chain. Although, the above-mentioned features are evident from our numerical results based on the 2D p-wave superconductor. In Fig. 8(a), we depict the LDOS at $E = 0$ in L_x-L_y plane choosing $B_0 = 0.0$ and $\mu = 2.0t$. In absence of any spin chain, the system is a purely 2D p-wave superconductor where MEMs appear and it is also reflected in the corresponding eigenvalue spectrum [see Fig. 8(e)]. On the other hand, at any intermediate values of μ and B_0, the MZMs hybridize with the MEMs as shown via LDOS [Figs. 8(b) and 8(c)] and the corresponding eigenvalue spectrum [Figs. 8(f) and 8(g)]. Further, MEMs disappear when $\mu = 4.0t$ and $B_0 = 5.0t$, only MZMs present and localized at the two ends of the chain [see Fig. 8(d)]. In this case, we obtain gapped eigenvalue spectrum and only two localized MZMs appear at exactly $E = 0$ [see Fig. 8(h)]. In the above cases, we fix the spiral wave vector at $G_s = 0.5$, i.e., the chain is in the topological regime.

As we start increasing G_s, the MZMs are gradually destroyed by the modulation of the spiral wave vector. It is clear from Fig. 9 that G_s drives the system from topological superconductor to trivial superconductor (s-wave like) within the magnetic spin chain (Shiba band). Note that the magnitude of $E = 0$ LDOS (unnormalized) is vanishingly small in Fig. 9(d) due to the absence of any zero-energy state in the trivial phase

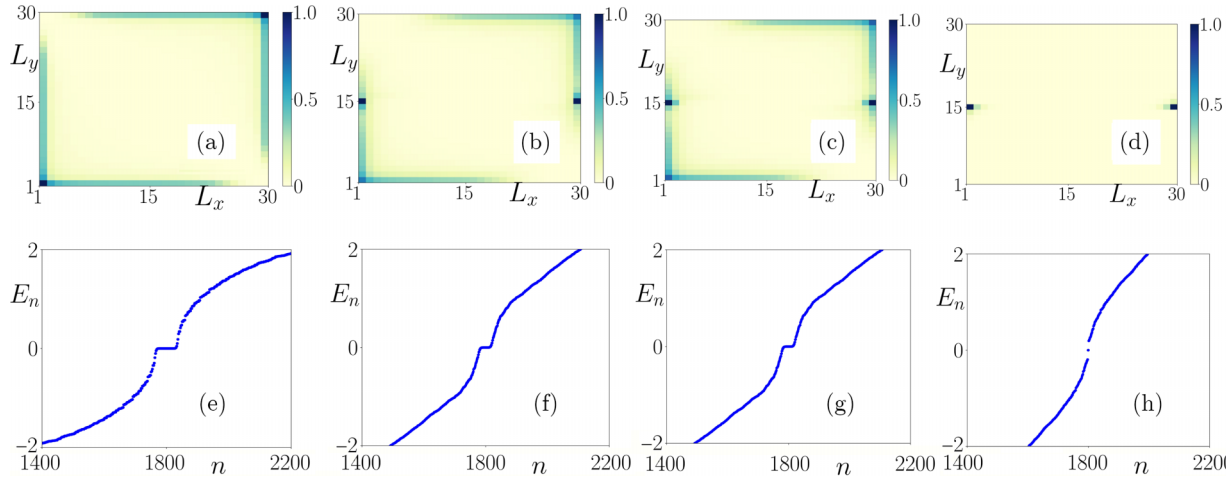

FIG. 8. (a), (b), (c), (d) Correspond to LDOS (at $E = 0$) in L_x-L_y plane for four different combinations of the parameters (i) $\mu = 2.0t$, $B_0 = 0.0$, (ii) $\mu = 3.0t$, $B_0 = 3.0t$, (iii) $\mu = 3.0t$, $B_0 = 4.0t$, and (iv) $\mu = 4.0t$, $B_0 = 5.0t$, respectively. (e), (f), (g), (h) Correspond to the eigenvalue spectrum for the same parameter regime, respectively. The other remaining parameters take the value $G_s = 0.5$ and $\Delta_p = t$.

as shown in Fig. 9(h). Therefore, when the chain is in the trivial regime, neither MEMs nor MZMs appear in the system.

V. SUMMARY AND CONCLUSIONS

To summarize, in this paper, we consider a 1D chain of magnetic impurities placed on a p-wave unconventional superconducting substrate and discuss the effect of different spin textures on the topological superconducting phase. First, we numerically analyze various 1D SS configurations by varying both G_s and G_h (controlling parameters for changing θ_l and ϕ_l) as the general case. We find that the effect of p-wave pairing gradually becomes weaker while an effective s-wave pairing is simultaneously generated, giving rise to a trivial superconducting phase at $G_h, G_s = (\pi, \pi)$. This is also reflected in the zero-energy LDOS behavior when it is calculated at the ends of the finite chain. If we continuously increase the pitch vectors of the SS by changing (G_h, G_s) until (π, π), then the Majorana peak height in the LDOS slowly decreases and eventually vanishes at (π, π). Hence, we find that the reason behind the complete destruction of MZMs is the formation of an effective s-wave pairing gap. Moreover, we analyze the gap structure $|E_2 - E_1|/\Delta_0$ in $G_s - G_h$ plane to find the gap closing points in the parameter phase. Interestingly, considering the Néel-type SS configuration ($G_h = 0, G_s \neq 0$), we compute the topological winding number W_n and show that sharp topological phase transition takes place around $G_{s1} = 2.5$ and $G_{s2} = 3.7$ where the band gap $|E_2 - E_1|$ closes. In order to have a better understanding of this phenomenon, we analyze this Néel-type rotation ($G_h = 0, G_s \neq 0$) further in both numerical and analytical model studies. Interestingly, we find that the rotation of magnetic impurity spins in the chain and p-wave superconductivity generates an effective s-wave superconducting phase at $G_s = \pi$, i.e., when the impurity spins form an antiferromagnetic spin chain. Thus, one can realize a phase transition from topological to trivial

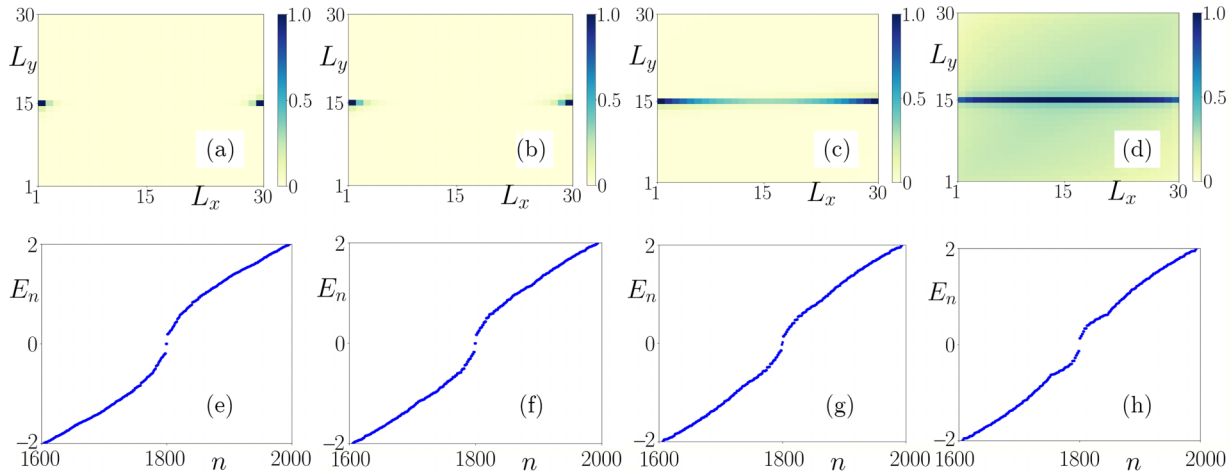

FIG. 9. (a), (b), (c), (d) Correspond to LDOS ($E = 0$) in L_x-L_y plane for four different values of the spiral wave vector $G_s = 0.5, 1.57, 2.4, 3.14$, respectively. (e), (f), (g), (h) Correspond to the eigenvalue spectrum for the same values of G_s, respectively. We choose the remaining parameter values as $\mu = 4.0t$, $B_0 = 5.0t$, $\Delta_p = t$.

superconductor in which the signature of MZMs vanishes in LDOS. In our analytical model, we begin from a low-energy model of a chain of magnetic impurities in the presence of p-wave superconducting pairing and obtain an analytical expression of the effective pairing $\tilde{\Delta}_{ij}^{\text{eff}}$. We also calculate the total DOS from our analytically obtained energy spectrum ϵ_k at $G_s = \pi$. This exhibits a conventional s-wave-like behavior which qualitatively matches with our numerical results. Moreover, we show that the nontopological Shiba bands (within $-\Delta_p$ to Δ_p) oscillate with the spiral wave vector G_s, when the system reaches to the trivial s-wave superconducting phase. Such kind of oscillation can be obtained when magnetic impurities are placed on an s-wave superconductor. We also consider a 2D p-wave superconductor and show via the LDOS and eigenvalue spectrum that initially MZMs can hybridize with the MEMs. However, even when the magnetic chain is in the topological regime, MEMs disappear at some critical value of the chemical potential μ and exchange coupling strength $B_0 = JS$ and only MZMs survive. These MZMs also disappear when the chain is in the trivial regime with further modulation of the SS wave vector G_s.

Experimental realization of topological Shiba bands in atomic spin chains has been reported in very recent experiments [62,66,89–93]. In those experiments, different transition metals like Fe [91], Mn [93], etc., have been designed as a chain of magnetic impurity atoms on the surface of conventional s-wave superconducting substrates like Pb (110), Nb (110) [66,91], etc. In such systems, the value of the s-wave pairing gap (e.g., Nb) is approximately $\Delta_s \sim 1.52$ meV [91] and experiments have been performed at low temperatures (1.4–1.6 K) [66]. They have observed the Majorana ZBP in topological Shiba bands via (dI/dV) measurement with different positions of the scanning tunneling microscope tip [66,91]. Therefore, given the so far experimental progress in this research field, we believe that our theoretical model proposal is timely and may be possible to realize in future experiments based on p superconductors engineered in materials, e.g., heterostructures by growing a magnetic layer on a Rashba superconductor [67], doped topological insulator [68–70], etc. Furthermore, the smooth variation of G can be attributed to the high tunability of RKKY exchange tensor and magnetocrystalline anisotropy energy by various routes [78,81–83].

ACKNOWLEDGMENTS

A.K.N. and A.S. acknowledge the support from the Department of Atomic Energy, Government of India. P.C. acknowledges S. Saha, A. K. Ghosh, and D. Mandal for useful discussions.

APPENDIX A: OSCILLATION OF THE SHIBA BANDS IN CASE OF s-WAVE SUPERCONDUCTOR

Here, we discuss the nature of the Shiba bands when magnetic impurities are placed on a conventional s-wave superconductor. It is evident from Figs. 10(a) and Fig. 10(b) that Shiba bands are formed within $-\Delta_s$ to Δ_s and they are nontopological in nature when $G_s = 0$. We obtain the oscillation of the Shiba bands with respect to G_s when the Shiba states corresponding to the individual impurity spin interferes with each other. It is an important observation for the formation of

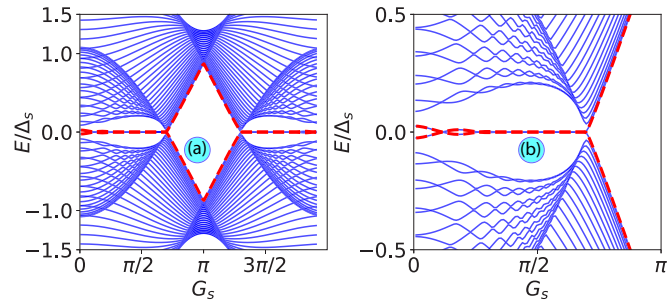

FIG. 10. (a) Band spectrum (E) is shown as a function of spiral wave vector (G_s) within the energy range $-1.5\Delta_s$ to $1.5\Delta_s$ considering purely s-wave pairing. Here, we choose $\mu = 4t$, $B_0 = 5t$, $\Delta_s = 1.0t$. (b) Close view of the energy spectrum (within the range $-0.5\Delta_s \rightarrow 0.5\Delta_s$) is depicted when G_s varies from $0 \rightarrow \pi$.

s-wave superconductor as mentioned in Fig. 5(a) of the main text. It is evident from Fig. 10(a) that such oscillation of Shiba band persists until $G_s \leqslant \pi/2$, i.e., within the trivial regime. When $G_s \geqslant \pi/2$, the system enters into the topological superconducting regime due to the formation of an effective p-wave gap and such oscillation of the Shiba bands disappears [see Fig. 10(b) for more clarity].

APPENDIX B: ANALYTICAL CALCULATION OF THE EFFECTIVE PAIRING GAP BASED ON LOW-ENERGY EFFECTIVE MODEL

In order to support our numerical results based on the lattice model [Eq. (1)], we also carry out analytical calculation considering low-energy BdG Hamiltonian that describes magnetic impurities on a p-wave superconductor. Our continuum Hamiltonian can be written as

$$H = \xi_k \tau_z - J \sum_j \vec{S}_j \cdot \vec{\sigma}\, \delta(x - x_j) + \Delta_p k \tau_y, \tag{B1}$$

where $\xi_k = \frac{k^2}{2m} - \mu$, k is the momentum along the 1D chain, and Δ_p is the superconducting gap. Particle hole and spin degrees of freedom can be expressed in terms of Pauli matrices τ and σ, respectively. The BdG Hamiltonian can be expressed in terms of Nambu basis $\Phi = (\phi_\uparrow, \phi_\downarrow, \phi_\downarrow^\dagger, -\phi_\uparrow^\dagger)$.

At first, we calculate the eigenvalues and eigenvectors for a single magnetic impurity placed on a p-wave superconductor. The motivation for this part is to understand the spinors that are needed for our final calculation of the multiple impurities. For arbitrary orientation of the single-impurity spin, our Hamiltonian reads as

$$H = \xi_k \tau_z - J\vec{S} \cdot \vec{\sigma} + \Delta_p k \tau_y. \tag{B2}$$

The eigenvalues of Eq. (B2) are

$$\lambda_1 = -\left(JS + \sqrt{\xi_k^2 + \Delta_p^2 k^2}\right), \tag{B3}$$

$$\lambda_2 = JS - \sqrt{\xi_k^2 + \Delta_p^2 k^2}, \tag{B4}$$

$$\lambda_3 = -\left(JS - \sqrt{\xi_k^2 + \Delta_p^2 k^2}\right), \tag{B5}$$

$$\lambda_4 = \left(JS + \sqrt{\xi_k^2 + \Delta_p^2 k^2}\right). \tag{B6}$$

The corresponding BdG spinors of the eigenvectors can be written as

$$\alpha_1 = \begin{pmatrix} \frac{i\left(-\xi_k+\sqrt{\xi_k^2+\Delta_p^2k^2}\right)}{k\Delta_p}\cos\left(\frac{\theta}{2}\right) \\ -\frac{i\left(\xi_k-\sqrt{\xi_k^2+\Delta_p^2k^2}\right)}{k\Delta_p}e^{i\phi}\sin\left(\frac{\theta}{2}\right) \\ \cos\frac{\theta}{2} \\ e^{i\phi}\sin\left(\frac{\theta}{2}\right) \end{pmatrix}, \tag{B7}$$

$$\alpha_2 = \begin{pmatrix} \frac{i\left(\xi_k-\sqrt{\xi_k^2+\Delta_p^2k^2}\right)}{k\Delta_p}e^{-i\phi}\sin\left(\frac{\theta}{2}\right) \\ -\frac{i\left(\xi_k-\sqrt{\xi_k^2+\Delta_p^2k^2}\right)}{k\Delta_p}\cos\left(\frac{\theta}{2}\right) \\ -e^{-i\phi}\sin\frac{\theta}{2} \\ \cos(\frac{\theta}{2}) \end{pmatrix}, \tag{B8}$$

$$\alpha_3 = \begin{pmatrix} -\frac{i\left(\xi_k+\sqrt{\xi_k^2+\Delta_p^2k^2}\right)}{k\Delta_p}\cos\left(\frac{\theta}{2}\right) \\ -\frac{i\left(\xi_k+\sqrt{\xi_k^2+\Delta_p^2k^2}\right)}{k\Delta_p}e^{i\phi}\sin\left(\frac{\theta}{2}\right) \\ \cos\frac{\theta}{2} \\ e^{i\phi}\sin(\frac{\theta}{2}) \end{pmatrix}, \tag{B9}$$

$$\alpha_4 = \begin{pmatrix} \frac{i\left(\xi_k+\sqrt{\xi_k^2+\Delta_p^2k^2}\right)}{k\Delta_p}e^{-i\phi}\sin\left(\frac{\theta}{2}\right) \\ -\frac{i\left(\xi_k+\sqrt{\xi_k^2+\Delta_p^2k^2}\right)}{k\Delta_p}\cos\left(\frac{\theta}{2}\right) \\ -e^{-i\phi}\sin\frac{\theta}{2} \\ \cos\left(\frac{\theta}{2}\right) \end{pmatrix}. \tag{B10}$$

Under the approximation $\xi_k \ll \Delta_p$, these spinors take the form

$$\psi_1 = \begin{pmatrix} i\cos\left(\frac{\theta}{2}\right) \\ ie^{i\phi}\sin\left(\frac{\theta}{2}\right) \\ \cos\frac{\theta}{2} \\ e^{i\phi}\sin\left(\frac{\theta}{2}\right) \end{pmatrix}, \quad \psi_3 = \begin{pmatrix} -ie^{-i\phi}\sin\left(\frac{\theta}{2}\right) \\ i\cos\left(\frac{\theta}{2}\right) \\ -e^{-i\phi}\sin\frac{\theta}{2} \\ \cos\left(\frac{\theta}{2}\right) \end{pmatrix}, \tag{B11}$$

$$\psi_2 = \begin{pmatrix} -i\cos\left(\frac{\theta}{2}\right) \\ -ie^{i\phi}\sin\left(\frac{\theta}{2}\right) \\ \cos\frac{\theta}{2} \\ e^{i\phi}\sin\left(\frac{\theta}{2}\right) \end{pmatrix}, \quad \psi_4 = \begin{pmatrix} ie^{-i\phi}\sin\left(\frac{\theta}{2}\right) \\ -i\cos\left(\frac{\theta}{2}\right) \\ -e^{-i\phi}\sin\frac{\theta}{2} \\ \cos\left(\frac{\theta}{2}\right) \end{pmatrix}. \tag{B12}$$

The eigenvectors of $\boldsymbol{\sigma}\cdot\boldsymbol{S}$ are

$$|\uparrow\rangle = \begin{pmatrix} \cos\left(\frac{\theta}{2}\right) \\ e^{i\phi}\sin\left(\frac{\theta}{2}\right) \end{pmatrix}, \quad |\downarrow\rangle = \begin{pmatrix} e^{-i\phi}\sin\left(\frac{\theta}{2}\right) \\ -\cos\left(\frac{\theta}{2}\right) \end{pmatrix}. \tag{B13}$$

Hence, we can write the BdG spinors in terms of the eigenstates of $\boldsymbol{\sigma}\cdot\boldsymbol{S}$ as

$$\psi_1 = \begin{pmatrix} i|\uparrow\rangle \\ |\uparrow\rangle \end{pmatrix}, \quad \psi_3 = \begin{pmatrix} -i|\downarrow\rangle \\ -|\downarrow\rangle \end{pmatrix}, \tag{B14}$$

$$\psi_2 = \begin{pmatrix} -i|\uparrow\rangle \\ |\uparrow\rangle \end{pmatrix}, \quad \psi_4 = \begin{pmatrix} i|\downarrow\rangle \\ -|\downarrow\rangle \end{pmatrix}. \tag{B15}$$

As for p-wave superconductor the constituent quasiparticles exhibit symmetric spin, i.e., triplet pairing, therefore, one has to choose the spatial wave functions as

$$\psi_1(r_j) = \begin{pmatrix} i|\uparrow,j\rangle \\ |\uparrow,j\rangle \end{pmatrix}, \quad \psi_2(r_j) = \begin{pmatrix} -i|\uparrow,j\rangle \\ |\uparrow,j\rangle \end{pmatrix}. \tag{B16}$$

Hence, for multiple impurities we start from the Schrödinger equation $H\psi(x) = E\psi(x)$. Now, following Ref. [38] we can write from Eq. (B1),

$$[E-\xi_k\tau_z-\Delta_pk\tau_y]\psi(x) = -JS\sum_j \hat{S}_j\cdot\vec{\sigma}\,\delta(x-x_j)\psi(x). \tag{B17}$$

Thus, one can further obtain

$$\begin{aligned}\psi(x_i) =& -JS\sum_j\int\frac{dk}{2\pi}\frac{e^{ik(x_i-x_j)}}{[E-\xi_k\tau_z-\Delta_pk\tau_y]}\hat{S}_j\cdot\vec{\sigma}\,\psi(x_j) \\ =& -JS\sum_j\int\frac{dk}{2\pi}\begin{pmatrix} \frac{E+\xi_k}{E^2-\xi_k^2-\Delta_k^2k^2} & \frac{-i\Delta_kk}{E^2-\xi_k^2-\Delta_k^2k^2} \\ \frac{i\Delta_kk}{E^2-\xi_k^2-\Delta_k^2k^2} & \frac{E-\xi_k}{E^2-\xi_k^2-\Delta_k^2k^2}\end{pmatrix} \\ &\times e^{ik(x_i-x_j)}\hat{S}_j\cdot\vec{\sigma}\,\psi(x_j).\end{aligned} \tag{B18}$$

From Eq. (B18), we can further find

$$\psi(x_i) = -\sum_j J_E(|x_i-x_j|)\hat{S}_j\cdot\vec{\sigma}\,\psi(x_j), \tag{B19}$$

where

$$\begin{aligned}J_E(|x_i-x_j|) &= J_E(x_{ij}) \\ &= f_E^{(1)}(x_{i,j})\mathbb{I} + f_E^{(2)}(x_{i,j})\tau_z + f_E^{(3)}(x_{i,j})\tau_y\end{aligned} \tag{B20}$$

and

$$\begin{aligned}f_E^{(1)}(x_{ij}) &= JS\int\frac{dk}{2\pi}\frac{Ee^{ikx_{ij}}}{E^2-\xi_k^2-\Delta_k^2k^2}, \\ f_E^{(2)}(x_{ij}) &= JS\int\frac{dk}{2\pi}\frac{\xi_ke^{ikx_{ij}}}{E^2-\xi_k^2-\Delta_k^2k^2}, \\ f_E^{(3)}(x_{ij}) &= JS\int\frac{dk}{2\pi}\frac{\Delta_kke^{ikx_{ij}}}{E^2-xi_k^2-\Delta_k^2k^2}.\end{aligned} \tag{B21}$$

Afterwards, we linearize the spectrum around the Fermi momentum and thus obtain $\xi_k = V_F(k-k_F)$. Here V_F and k_F are the Fermi velocity and Fermi momentum, respectively. Under this approximation, the results of the integrals are given by (see Ref. [85])

$$\begin{aligned}f_E^{(1)}(x) &= -\frac{E}{V_F}\frac{JS}{1+\tilde{\Delta}_p^2}\frac{\cos(k_F'x)}{\omega(E)}e^{-\frac{\omega(E)x}{V_F}}, \\ f_E^{(2)}(x) &= \frac{1}{V_F}\frac{JS}{1+\tilde{\Delta}_p^2}\left[\frac{\gamma\Delta_t}{\omega(E)}\cos\left(k_F'x\right)+\sin\left(k_F'x\right)\right]e^{-\frac{\omega(E)x}{V_F}}, \\ f_E^{(3)}(x) &= -\frac{i}{V_F}\frac{\tilde{\Delta}_pJS}{1+\tilde{\Delta}_p^2}\left[\frac{k_F'V_F}{\omega(E)}\sin\left(k_F'x\right)+\mathrm{sgn}(x)\cos\left(k_F'x\right)\right] \\ &\quad\times e^{-\frac{\omega(E)x}{V_F}},\end{aligned} \tag{B22}$$

where $k_F' = \frac{k_F}{\sqrt{1+\tilde{\Delta}_p^2}}$, $\tilde{\Delta}_p = \frac{\Delta_p}{V_F}$, $\omega(E) = \frac{\sqrt{\Delta_t^2-E^2}}{\sqrt{1+\tilde{\Delta}_p^2}}$, $\Delta_t = \frac{\Delta_pk_F}{\sqrt{1+\tilde{\Delta}_p^2}}$, $\gamma = \frac{\tilde{\Delta}_p}{\sqrt{1+\tilde{\Delta}_p^2}}$ as introduced in the main text also.

From Eq. (B19) we can write

$$\psi(x_i) + J_E(0)\hat{S}_i \cdot \vec{\sigma}\,\psi(x_i) = -\sum_{j\neq i} J_E(|x_i - x_j|)\hat{S}_j \cdot \vec{\sigma}\,\psi(x_j). \tag{B23}$$

Therefore, at $|x_i - x_j| = 0$, these functions become

$$f_E^{(1)}(0) = -\frac{JS}{V_F}\frac{E}{\sqrt{1+\tilde{\Delta}_p^2}}\frac{1}{\sqrt{\Delta_t^2 - E^2}},$$
$$f_E^{(2)}(0) = \frac{JS}{V_F}\frac{\gamma\Delta_t}{\sqrt{1+\tilde{\Delta}_p^2}}\frac{1}{\sqrt{\Delta_t^2 - E^2}},$$
$$f_E^{(3)}(x) = 0. \tag{B24}$$

We can define the impurity strength in terms of a new parameter $\alpha = JS/(V_F\sqrt{1+\tilde{\Delta}_p^2})$. We further assume that impurities are sufficiently dilute such that the resulting impurity band remains well within the superconducting gap, i.e., $\Delta_t \gg E$. Using Eq. (B24) and substituting $E = 0, \alpha = 1/\gamma$ in the right-hand side of Eq. (B23), we obtain (following Ref. [85])

$$\left[\hat{S}_i \cdot \vec{\sigma} - \left(\frac{\alpha E}{\Delta_t} - \alpha\gamma\tau_z\right)\right]\psi(x_i) = -\sum_{j\neq i}\left[f_0^{(2)}(x_{ij})\tau_z + f_0^{(3)}(x_{ij})\tau_y\right](\hat{S}_i \cdot \vec{\sigma})(\hat{S}_j \cdot \vec{\sigma})\psi(x_j). \tag{B25}$$

Hence, Eq. (B25) can be written as

$$\tilde{H}_{\text{eff}}\phi = E\phi. \tag{B26}$$

Now projecting Eq. (B16) into (B25), we can find the diagonal and off-diagonal elements of H_{eff} as

$$\tilde{h}_{ij}^{\text{eff}} = (\epsilon_0/2)\delta_{ij} + (1-\delta_{ij}) \times [k_F'\Delta_p \sin(k_F'|x_{ij}|) + \gamma\Delta_t \text{sgn}(x_{ij})\cos(k_F'x_{ij})] \times e^{-\frac{|x_{ij}|}{\xi_0}}\langle\uparrow, i|\,|\uparrow, j\rangle \tag{B27}$$

and

$$(\tilde{\Delta}^{\text{eff}})_{ij} = -(\epsilon_0/2)\delta_{ij} - (1-\delta_{ij}) \times \left[\frac{\Delta_t}{\sqrt{1+\tilde{\Delta}_p^2}}\sin(k_F'|x_{ij}|) + \gamma\Delta_t\cos(k_F'x_{ij})\right] \times e^{-\frac{|x_{ij}|}{\xi_0}}\langle\uparrow, i|\,|\uparrow, j\rangle, \tag{B28}$$

where $\epsilon_0 = 2\Delta_t/\alpha$ denotes the Shiba bound-state energy for a single magnetic impurity in the deep Shiba limit and $\xi_0 = V_F/\omega(0)$ is the phase coherence length for a p-wave superconductor. Here, $\tilde{\Delta}_{ij}^{\text{eff}}$ denotes the effective pairing gap in real space which we have mentioned in the main text [see Eq. (7)].

Therefore, considering Néel-type rotation of the magnetic impurities, i.e., $\phi_i = 0$ and $\theta_i = G_s ja$ (j is the lattice site index and a is the lattice spacing), one can obtain

$$\langle\uparrow, i|\,|\uparrow, j\rangle = \cos(G_s x_{ij}/2)$$

and

$$\langle\uparrow, i|\,|\downarrow, j\rangle = -\sin(G_s x_{ij}/2).$$

Hence, the effective k-space 2×2 BdG Hamiltonian reads as

$$H_k = \begin{pmatrix} h_k & \Delta_k \\ \Delta_k^* & -h_{-k}^* \end{pmatrix}, \tag{B29}$$

where

$$h_k = \sum_j (\tilde{h}^{\text{eff}})_{ij} e^{ikx_{ij}}, \tag{B30}$$
$$\Delta_k = \sum_j (\tilde{\Delta}^{\text{eff}})_{ij} e^{ikx_{ij}}. \tag{B31}$$

Inserting Eqs. (B27) and (B28) into the above equations, we finally obtain Eqs. (9) and (10) which we have introduced in the main text to explain our analytical results.

APPENDIX C: ANALYTICAL SOLUTION OF TOPOLOGICAL PHASE BOUNDARY FOR OUR 1D LATTICE MODEL HAMILTONIAN

As the tight-binding model [Eq. (1) in our main text] does not respect translational symmetry, hence, we cannot directly perform Fourier transform to obtain a spectrum in k space. Thus, following Ref. [35], we transform our Hamiltonian to the Majorana basis in order to diagonalize it in momentum space. Under the new basis $m_k = (m_{k,1,\uparrow}, m_{k,1,\downarrow}, m_{k,2,\uparrow}, m_{k,2,\downarrow})$, our k-space Hamiltonian can be written for the Néel-type rotation as

$$H(k) = \frac{i}{4}\sum_k m_k^\dagger h(k) m_k, \tag{C1}$$

where nonzero elements of Eq. (C1) are

$$h_{13} = (2t + \Delta_p)\alpha\,\cos(k) + B_0 - \mu = h_{31}^*, \tag{C2}$$
$$h_{14} = 2it\beta\,\sin(k) - \Delta_p\beta\,\cos(k) = h_{41}^*, \tag{C3}$$
$$h_{23} = -2it\beta\,\sin(k) + \Delta_p\beta\,\cos(k) = h_{32}^*, \tag{C4}$$
$$h_{24} = (2t + \Delta_p)\alpha\,\cos(k) - B_0 - \mu = h_{42}^*. \tag{C5}$$

For $k = \pi$, the eigenvalues of the above Hamiltonian [Eq. (C1)] can be written as

$$E = \pm\frac{1}{4}\left[B_0 \pm \sqrt{(\mu + 2\alpha t)^2 + \Delta_p^2(\alpha^2+\beta^2) + 2\alpha\Delta_p(\mu + 2\alpha t)}\right], \tag{C6}$$

where $\alpha = \cos(G_s/2)$ and $\beta = \sin(G_s/2)$. In presence of a p-wave superconductor, the system is initially topological and after a critical value of the exchange field $B_0 = JS$, it goes to a nontopological phase. We obtain this critical exchange field from the gap-closing condition of the two minimum bands. From Eq. (C6) we obtain

$$|B_{c1}| = \sqrt{(\mu + 2\alpha t)^2 + \Delta_p^2(\alpha^2+\beta^2) + 2\alpha\Delta_p(\mu + 2\alpha t)}. \tag{C7}$$

On the other hand, for $k = 0$ the eigenvalues of the Hamiltonian become

$$E = \pm\frac{1}{4}\left[B_0 \pm \sqrt{(\mu - 2\alpha t)^2 + \Delta_p^2(\alpha^2 + \beta^2) - 2\alpha\Delta_p(\mu - 2\alpha t)}\right]. \tag{C8}$$

Similarly, from the gap closing condition (considering the lowest two bands) the critical exchange field becomes

$$|B_{c2}| = \sqrt{(\mu - 2\alpha t)^2 + \Delta_p^2(\alpha^2 + \beta^2) - 2\alpha\Delta_p(\mu - 2\alpha t)}. \tag{C9}$$

Hence, considering the parameters values $\mu = 4t$, $B_0 = 5t$, $\Delta_p = t$ and employing Eqs. (C7) and (C9) we obtain $G_{s1} = 2.526\,39$ and $G_{s2} = 3.7568$. This matches well with the numerically obtained gap closing points as well as sharp jump of the topological invariant [see Fig. 3(b)].

Out of four cases, here we present the calculation for Néel-type rotation ($\theta_l = G_s l$ and $\phi_l = 0$) only. For the other two cases, Bloch-type ($\theta_l = G_s l, \phi_l = \pi/2$) and conical-spin spiral ($\theta_l = \pi/2, \phi_l = G_h l$), our results remain the same.

[1] D. J. Thouless, M. Kohmoto, M. P. Nightingale, and M. den Nijs, Quantized Hall Conductance in a Two-Dimensional Periodic Potential, Phys. Rev. Lett. **49**, 405 (1982).

[2] C. L. Kane and E. J. Mele, Quantum Spin Hall Effect in Graphene, Phys. Rev. Lett. **95**, 226801 (2005).

[3] C. L. Kane and E. J. Mele, Z2 Topological Order and the Quantum Spin Hall Effect, Phys. Rev. Lett. **95**, 146802 (2005).

[4] B. A. Bernevig, T. L. Hughes, and S.-C. Zhang, Quantum spin hall effect and topological phase transition in HgTe quantum wells, Science **314**, 1757 (2006).

[5] X.-L. Qi and S.-C. Zhang, Topological insulators and superconductors, Rev. Mod. Phys. **83**, 1057 (2011).

[6] M. König, S. Wiedmann, C. Brüne, A. Roth, H. Buhmann, L. W. Molenkamp, X.-L. Qi, and S.-C. Zhang, Quantum spin hall insulator state in hgte quantum wells, Science **318**, 766 (2007).

[7] M. Kohmoto, Topological invariant and the quantization of the hall conductance, Ann. Phys. **160**, 343 (1985).

[8] *Topological Insulators*, Contemporary Concepts of Condensed Matter Science, Vol. 6, edited by M. Franz and L. Molenkamp (Elsevier, Amsterdam, 2013), Chap. 1, pp. 3–34.

[9] J. E. Moore and L. Balents, Topological invariants of time-reversal-invariant band structures, Phys. Rev. B **75**, 121306(R) (2007).

[10] L. Fu, C. L. Kane, and E. J. Mele, Topological Insulators in Three Dimensions, Phys. Rev. Lett. **98**, 106803 (2007).

[11] R. Roy, Topological phases and the quantum spin hall effect in three dimensions, Phys. Rev. B **79**, 195322 (2009).

[12] Y. Ando, Topological insulator materials, J. Phys. Soc. Jpn. **82**, 102001 (2013).

[13] L. Fu and C. L. Kane, Topological insulators with inversion symmetry, Phys. Rev. B **76**, 045302 (2007).

[14] J. C. Y. Teo, L. Fu, and C. L. Kane, Surface states and topological invariants in three-dimensional topological insulators: Application to $Bi_{1-x}Sb_x$, Phys. Rev. B **78**, 045426 (2008).

[15] X.-L. Qi, T. L. Hughes, and S.-C. Zhang, Topological field theory of time-reversal invariant insulators, Phys. Rev. B **78**, 195424 (2008).

[16] M. M. Hosen, K. Dimitri, A. K. Nandy, A. Aperis, R. Sankar, G. Dhakal, P. Maldonado, F. Kabir, C. Sims, F. Chou, D. Kaczorowski, T. Durakiewicz, P. M. Oppeneer, and M. Neupane, Distinct multiple fermionic states in a single topological metal, Nat. Commun. **9**, 3002 (2018).

[17] G. Dhakal, F. Kabir, A. K. Nandy, A. Aperis, A. P. Sakhya, S. Pradhan, K. Dimitri, C. Sims, S. Regmi, M. M. Hosen, Y. Liu, L. Persaud, D. Kaczorowski, P. M. Oppeneer, and M. Neupane, Observation of anisotropic dirac cones in the topological material Ti_2Te_2P, Phys. Rev. B **106**, 125124 (2022).

[18] A. Altland and M. R. Zirnbauer, Nonstandard symmetry classes in mesoscopic normal-superconducting hybrid structures, Phys. Rev. B **55**, 1142 (1997).

[19] A Yu Kitaev, Unpaired Majorana fermions in quantum wires, Phys. Usp. **44**, 131 (2001).

[20] A. Kitaev, Periodic table for topological insulators and superconductors, in *Advances in theoretical physics: Landau Memorial Conference*, edited by Vladimir Lebedev and Mikhail Feigel'man (American Institute of Physics, Melville, NY, 2009), Vol. 1134, pp. 22–30.

[21] N. Read and D. Green, Paired states of fermions in two dimensions with breaking of parity and time-reversal symmetries and the fractional quantum hall effect, Phys. Rev. B **61**, 10267 (2000).

[22] L. Fu and C. L. Kane, Superconducting Proximity Effect and Majorana Fermions at the Surface of a Topological Insulator, Phys. Rev. Lett. **100**, 096407 (2008).

[23] M. Sato, Non-abelian statistics of axion strings, Phys. Lett. B **575**, 126 (2003).

[24] B. Simon, Holonomy, the Quantum Adiabatic Theorem, and Berry's Phase, Phys. Rev. Lett. **51**, 2167 (1983).

[25] J. E. Avron, R. Seiler, and B. Simon, Homotopy and Quantization in Condensed Matter Physics, Phys. Rev. Lett. **51**, 51 (1983).

[26] C. Nayak, S. H. Simon, A. Stern, M. Freedman, and S. D. Sarma, Non-abelian anyons and topological quantum computation, Rev. Mod. Phys. **80**, 1083 (2008).

[27] Y. Oreg, G. Refael, and F. von Oppen, Helical Liquids and Majorana Bound States in Quantum Wires, Phys. Rev. Lett. **105**, 177002 (2010).

[28] R. M. Lutchyn, J. D. Sau, and S. Das Sarma, Majorana Fermions and a Topological Phase Transition in Semiconductor-Superconductor Heterostructures, Phys. Rev. Lett. **105**, 077001 (2010).

[29] V. Mourik, K. Zuo, S. M. Frolov, S. Plissard, E. Bakkers, and L. P. Kouwenhoven, Signatures of Majorana fermions in hybrid superconductor-semiconductor nanowire devices, Science **336**, 1003 (2012).

[30] A. Das, Y. Ronen, Y. Most, Y. Oreg, M. Heiblum, and H. Shtrikman, Zero-bias peaks and splitting in an Al – InAs nanowire topological superconductor as a signature of Majorana fermions, Nat. Phys. **8**, 887 (2012).

[31] L. P. Rokhinson, X. Liu, and J. K. Furdyna, The fractional ac josephson effect in a semiconductor-superconductor nanowire as a signature of Majorana particles, Nat. Phys. **8**, 795 (2012).

[32] A. D. K. Finck, D. J. Van Harlingen, P. K. Mohseni, K. Jung, and X. Li, Anomalous Modulation of a Zero-Bias Peak in a Hybrid Nanowire-Superconductor Device, Phys. Rev. Lett. **110**, 126406 (2013).

[33] S. M. Albrecht, A. P. Higginbotham, M. Madsen, F. Kuemmeth, T. S. Jespersen, J. Nygård, P. Krogstrup, and C. M. Marcus, Exponential protection of zero modes in majorana islands, Nature (London) **531**, 206 (2016).

[34] M. T. Deng, S. Vaitiekėnas, E. B. Hansen, J. Danon, M. Leijnse, K. Flensberg, J. Nygård, P. Krogstrup, and C. M. Marcus, Majorana bound state in a coupled quantum-dot hybrid-nanowire system, Science **354**, 1557 (2016).

[35] S. Nadj-Perge, I. K. Drozdov, B. A. Bernevig, and A. Yazdani, Proposal for realizing majorana fermions in chains of magnetic atoms on a superconductor, Phys. Rev. B **88**, 020407(R) (2013).

[36] T.-P. Choy, J. M. Edge, A. R. Akhmerov, and C. W. J. Beenakker, Majorana fermions emerging from magnetic nanoparticles on a superconductor without spin-orbit coupling, Phys. Rev. B **84**, 195442 (2011).

[37] S. Rex, I. V. Gornyi, and A. D. Mirlin, Majorana modes in emergent-wire phases of helical and cycloidal magnet-superconductor hybrids, Phys. Rev. B **102**, 224501 (2020).

[38] F. Pientka, L. I. Glazman, and F. von Oppen, Topological superconducting phase in helical Shiba chains, Phys. Rev. B **88**, 155420 (2013).

[39] F. Pientka, L. I. Glazman, and F. von Oppen, Unconventional topological phase transitions in helical Shiba chains, Phys. Rev. B **89**, 180505(R) (2014).

[40] N. Mohanta, S. Okamoto, and E. Dagotto, Skyrmion control of majorana states in planar josephson junctions, Commun. Phys. **4**, 163 (2021).

[41] J. Klinovaja, P. Stano, A. Yazdani, and D. Loss, Topological Superconductivity and Majorana Fermions in RKKY Systems, Phys. Rev. Lett. **111**, 186805 (2013).

[42] G. M. Andolina and P. Simon, Topological properties of chains of magnetic impurities on a superconducting substrate: Interplay between the Shiba band and ferromagnetic wire limits, Phys. Rev. B **96**, 235411 (2017).

[43] S. Hoffman, J. Klinovaja, and D. Loss, Topological phases of inhomogeneous superconductivity, Phys. Rev. B **93**, 165418 (2016).

[44] D. Sticlet and C. Morari, Topological superconductivity from magnetic impurities on monolayer $NbSe_2$, Phys. Rev. B **100**, 075420 (2019).

[45] J. D. Sau and E. Demler, Bound states at impurities as a probe of topological superconductivity in nanowires, Phys. Rev. B **88**, 205402 (2013).

[46] M. Mashkoori and A. Black-Schaffer, Majorana bound states in magnetic impurity chains: Effects of d-wave pairing, Phys. Rev. B **99**, 024505 (2019).

[47] M. Mashkoori, S. Pradhan, K. Björnson, J. Fransson, and A. M. Black-Schaffer, Identification of topological superconductivity in magnetic impurity systems using bulk spin polarization, Phys. Rev. B **102**, 104501 (2020).

[48] R. L. R. C. Teixeira, D. Kuzmanovski, A. M. Black-Schaffer, and L. G. G. V. D. da Silva, Enhanced majorana bound states in magnetic chains on superconducting topological insulator edges, Phys. Rev. B **102**, 165312 (2020).

[49] A. Theiler, K. Björnson, and A. M. Black-Schaffer, Majorana bound state localization and energy oscillations for magnetic impurity chains on conventional superconductors, Phys. Rev. B **100**, 214504 (2019).

[50] H.-Y. Hui, P. M. R. Brydon, J. D. Sau, S. Tewari, and S. D. Sarma, Majorana fermions in ferromagnetic chains on the surface of bulk spin-orbit coupled s-wave superconductors, Sci. Rep. **5**, 8880 (2015).

[51] V. Perrin, M. Civelli, and P. Simon, Identifying majorana bound states by tunneling shot-noise tomography, Phys. Rev. B **104**, L121406 (2021).

[52] M. H. Christensen, M. Schecter, K. Flensberg, B. M. Andersen, and J. Paaske, Spiral magnetic order and topological superconductivity in a chain of magnetic adatoms on a two-dimensional superconductor, Phys. Rev. B **94**, 144509 (2016).

[53] G. Sharma and S. Tewari, Yu-Shiba-Rusinov states and topological superconductivity in ising paired superconductors, Phys. Rev. B **94**, 094515 (2016).

[54] G. C. Ménard, C. Brun, R. Leriche, M. Trif, F. Debontridder, D. Demaille, D. Roditchev, P. Simon, and T. Cren, Yu-Shiba-Rusinov bound states versus topological edge states in Pb/Si(111), Eur. Phys. J. Special Topics **227** (2019).

[55] H. Shiba, Classical spins in superconductors, Prog. Theor. Phys. **40**, 435 (1968).

[56] O. Deb, S. Hoffman, D. Loss, and J. Klinovaja, Yu-Shiba-Rusinov states and ordering of magnetic impurities near the boundary of a superconducting nanowire, Phys. Rev. B **103**, 165403 (2021).

[57] F. von Oppen and K. J. Franke, Yu-Shiba-Rusinov states in real metals, Phys. Rev. B **103**, 205424 (2021).

[58] J. Ortuzar, S. Trivini, M. Alvarado, M. Rouco, J. Zaldivar, A. L. Yeyati, J. I. Pascual, and F. S. Bergeret, Yu-Shiba-Rusinov states in two-dimensional superconductors with arbitrary fermi contours, Phys. Rev. B **105**, 245403 (2022).

[59] C. W. J. Beenakker, Search for majorana fermions in superconductors, Annu. Rev. Condens. Matter Phys. **4**, 113 (2013).

[60] J. Alicea, New directions in the pursuit of majorana fermions in solid state systems, Rep. Prog. Phys. **75**, 076501 (2012).

[61] M. Leijnse and K. Flensberg, Introduction to topological superconductivity and majorana fermions, Semicond. Sci. Technol. **27**, 124003 (2012).

[62] D. Wang, J. Wiebe, R. Zhong, G. Gu, and R. Wiesendanger, Spin-Polarized Yu-Shiba-Rusinov States in an Iron-Based Superconductor, Phys. Rev. Lett. **126**, 076802 (2021).

[63] A. Yazdani, C. M. Howald, C. P. Lutz, A. Kapitulnik, and D. M. Eigler, Impurity-Induced Bound Excitations on the Surface of $Bi_2Sr_2CaCu_2O_8$, Phys. Rev. Lett. **83**, 176 (1999).

[64] A. Yazdani, B. A. Jones, C. P. Lutz, M. F. Crommie, and D. M. Eigler, Probing the local effects of magnetic impurities on superconductivity, Science **275**, 1767 (1997).

[65] A. Yazdani, Visualizing Majorana fermions in a chain of magnetic atoms on a superconductor, Phys. Scr. **2015**, 014012 (2015).

[66] S. Nadj-Perge, I. K. Drozdov, J. Li, H. Chen, S. Jeon, J. Seo, A. H. MacDonald, B. A. Bernevig, and A. Yazdani, Observation of majorana fermions in ferromagnetic atomic chains on a superconductor, Science **346**, 602 (2014).

[67] G. C. Ménard, S. Guissart, C. Brun, R. T. Leriche, M. Trif, F. Debontridder, D. Demaille, D. Roditchev, P. Simon, and T. Cren, Two-dimensional topological superconductivity in Pb/Co/Si(111), Nat. Commun. **8**, 2040 (2017).

[68] Y. S. Hor, A. J. Williams, J. G. Checkelsky, P. Roushan, J. Seo, Q. Xu, H. W. Zandbergen, A. Yazdani, N. P. Ong, and R. J. Cava, Superconductivity in $Cu_xBi_2Se_3$ and its Implications for Pairing in the Undoped Topological Insulator, Phys. Rev. Lett. **104**, 057001 (2010).

[69] L. Fu and E. Berg, Odd-Parity Topological Superconductors: Theory and Application to $Cu_xBi_2Se_3$, Phys. Rev. Lett. **105**, 097001 (2010).

[70] L. A. Wray, S. Xu, Y. Xia, D. Qian, A. V. Fedorov, H. Lin, A. Bansil, L. Fu, Y. S. Hor, R. J. Cava, and M. Z. Hasan, Spin-orbital ground states of superconducting doped topological insulators: A majorana platform, Phys. Rev. B **83**, 224516 (2011).

[71] V. Kaladzhyan, C. Bena, and P. Simon, Topology from triviality, Phys. Rev. B **97**, 104512 (2018).

[72] N. Sedlmayr and C. Bena, Visualizing majorana bound states in one and two dimensions using the generalized majorana polarization, Phys. Rev. B **92**, 115115 (2015).

[73] M. M. Vazifeh and M. Franz, Self-Organized Topological State with Majorana Fermions, Phys. Rev. Lett. **111**, 206802 (2013).

[74] A. K. Nandy, N. S. Kiselev, and S. Blügel, Interlayer Exchange Coupling: A General Scheme Turning Chiral Magnets into Magnetic Multilayers Carrying Atomic-Scale Skyrmions, Phys. Rev. Lett. **116**, 177202 (2016).

[75] C. Singh, V. Singh, G. Pradhan, V. Srihari, H. K. Poswal, R. Nath, A. K. Nandy, and A. K. Nayak, Pressure controlled trimerization for switching of anomalous hall effect in triangular antiferromagnet Mn_3Sn, Phys. Rev. Res. **2**, 043366 (2020).

[76] T. Kitagawa, E. Berg, M. Rudner, and E. Demler, Topological characterization of periodically driven quantum systems, Phys. Rev. B **82**, 235114 (2010).

[77] S. Tewari and J. D. Sau, Topological Invariants for Spin-Orbit Coupled Superconductor Nanowires, Phys. Rev. Lett. **109**, 150408 (2012).

[78] C. Singh, S. Jamaluddin, A. K. Nandy, M. Tokunaga, M. Avdeev, and A. K. Nayak, Higher order exchange driven non-coplanar magnetic state and large anomalous hall effects in electron doped kagome magnet Mn_3Sn, arXiv:2211.12722.

[79] G. Zheng, M. Wang, X. Zhu, C. Tan, J. Wang, S. Albarakati, N. Aloufi, M. Algarni, L. Farrar, M. Wu, Y. Yao, M. Tian, J. Zhou, and L. Wang, Tailoring Dzyaloshinskii-Moriya interaction in a transition metal dichalcogenide by dual-intercalation, Nat. Commun. **12**, 3639 (2021).

[80] T. Ma, A. K. Sharma, R. Saha, A. K. Srivastava, P. Werner, P. Vir, V. Kumar, C. Felser, and S. S. P. Parkin, Tunable magnetic antiskyrmion size and helical period from nanometers to micrometers in a D_{2d} heusler compound, Adv. Mater. **32**, 2002043 (2020).

[81] P.-J. Hsu, A. Finco, L. Schmidt, A. Kubetzka, K. von Bergmann, and R. Wiesendanger, Guiding Spin Spirals by Local Uniaxial Strain Relief, Phys. Rev. Lett. **116**, 017201 (2016).

[82] H. Yang, O. Boulle, V. Cros, A. Fert, and M. Chshiev, Controlling dzyaloshinskii-moriya interaction via chirality dependent atomic-layer stacking, insulator capping and electric field, Sci. Rep. **8**, 12356 (2018).

[83] A. A. Khajetoorians, M. Steinbrecher, M. Ternes, M. Bouhassoune, M. dos Santos Dias, S. Lounis, J. Wiebe, and R. Wiesendanger, Tailoring the chiral magnetic interaction between two individual atoms, Nat. Commun. **7**, 10620 (2016).

[84] A. A. Zyuzin and D. Loss, RKKY interaction on surfaces of topological insulators with superconducting proximity effect, Phys. Rev. B **90**, 125443 (2014).

[85] V. Kaladzhyan, C. Bena, and P. Simon, Asymptotic behavior of impurity-induced bound states in low-dimensional topological superconductors, J. Phys.: Condens. Matter **28**, 485701 (2016).

[86] B. Uchoa and A. H. Castro Neto, Superconducting States of Pure and Doped Graphene, Phys. Rev. Lett. **98**, 146801 (2007).

[87] K. L. Zhang, P. Wang, and Z. Song, Majorana flat band edge modes of topological gapless phase in 2D kitaev square lattice, Sci. Rep. **9**, 4978 (2019).

[88] P. Wang, S. Lin, G. Zhang, and Z. Song, Topological gapless phase in kitaev model on square lattice, Sci. Rep. **7**, 17179 (2017).

[89] F. Küster, S. Brinker, S. Lounis, S. S. P. Parkin, and P. Sessi, Long range and highly tunable interaction between local spins coupled to a superconducting condensate, Nat. Commun. **12**, 6722 (2021).

[90] F. Küster, S. Brinker, R. Hess, D. Loss, S. S. P. Parkin, J. Klinovaja, S. Lounis, and P. Sessi, Non-majorana modes in diluted spin chains proximitized to a superconductor, Proc. Natl. Acad. Sci. USA **119**, e2210589119 (2022).

[91] L. Schneider, P. Beck, T. Posske, D. Crawford, E. Mascot, S. Rachel, R. Wiesendanger, and J. Wiebe, Topological Shiba bands in artificial spin chains on superconductors, Nat. Phys. **17**, 943 (2021).

[92] P. Beck, L. Schneider, L. Rózsa, K. Palotás, A. Lászlóffy, L. Szunyogh, J. Wiebe, and R. Wiesendanger, Spin-orbit coupling induced splitting of Yu-Shiba-Rusinov states in antiferromagnetic dimers, Nat. Commun. **12**, 2040 (2021).

[93] L. Schneider, P. Beck, J. Neuhaus-Steinmetz, L. Rózsa, T. Posske, J. Wiebe, and R. Wiesendanger, Precursors of majorana modes and their length-dependent energy oscillations probed at both ends of atomic shiba chains, Nat. Nanotechnol. **17**, 384 (2022).